Effect of Annealing Temperature on the Structural, Magnetic, and Morphological Properties of Mg-Ni-Zn Ferrite Nanoparticles

Dattatray H. Bobade[1], Avinash T. Mane[2], Aparna T. Mane[3], Dinesh P. Shinde[3], *Sohail Bagwan[4]

[1]Department of Physics, C. T. Bora College, Shirur-412210, MS, India

[2]Department of Physics, Shankarrao Mohite Mahavidyalaya, Akluj, Solapur-413101, MS, India

[3]Department of Physics, K. B. P. Mahavidyalaya, Nano-Composite Research Laboratory, Pandharpur-413 304, Pandharpur, MS, India

[4]Department of Physics, Abeda Inamdar Senior College, Pune-411 001, MS, India

***Corresponding Author**

DOI: https://doi.org/10.51584/IJRIAS.2025.10060025

Received: 10 June 2025; Accepted: 16 June 2025; Published: 01 July 2025

ABSTRACT

The present study investigates the influence of annealing temperature on the structural, magnetic, and morphological properties of doped Mg-Ni-Zn ferrite nanoparticles synthesized via the sol-gel method. The nanoparticles were annealed at different temperatures ranging from 200°C to 600°C, and their phase composition, crystallinity, grain size, magnetic properties, and surface morphology were analysed using X-ray diffraction (XRD), Scanning Electron Microscopy (SEM), Energy-Dispersive X-ray Spectroscopy (EDS), and Vibrating Sample Magnetometry (VSM). The results indicate a significant enhancement in crystallinity and particle size with increasing temperature, while the magnetic properties exhibited a strong dependence on annealing conditions. The findings provide valuable insights into optimizing the annealing temperature for tailored ferrite properties in technological applications.

Keywords: Mg-Ni-Zn ferrite, sol-gel method, annealing temperature, structural properties, magnetic properties, morphological analysis, XRD, SEM, EDS, VSM.

INTRODUCTION

Ferrite nanoparticles have attracted significant attention in recent years due to their remarkable electrical, magnetic, and catalytic properties[1], [2], [3]. Among these, spinel ferrites with the general formula MFe_2O_4 (where M represents a divalent metal ion) are widely used in applications such as high-frequency transformers, microwave devices, sensors, and biomedical applications[4], [5], [6], [7]. Magnesium (Mg), Nickel (Ni), and Zinc (Zn) doped ferrites exhibit unique magnetic properties that can be tailored by varying synthesis conditions, chemical composition, and thermal treatments[8], [9], [10], [11], [12].

Ferrites are classified into three main types: spinel, hexagonal, and garnet ferrites. Among them, spinel ferrites are the most widely studied due to their superior structural stability, soft magnetic behaviour, and tenable electrical properties[13]. These materials exhibit high saturation magnetization, low coercivity, and excellent thermal and chemical stability, making them ideal for applications in data storage, electromagnetic interference (EMI) shielding, and magnetic resonance imaging (MRI) contrast agents[14], [15], [16]. Their dielectric properties also make them promising candidates for use in electronic components such as inductors and capacitors[17].

The unique magnetic behaviour of ferrites is attributed to their crystal structure, where metal cations occupy both tetrahedral and octahedral sites within the oxygen sublattice[18], [19]. The distribution of cations among these sites significantly influences the overall magnetic properties of the material. In doped Mg-Ni-Zn ferrites,

ISSN No. 2454-6194 | DOI: 10.51584/IJRIAS |Volume X Issue VI June 2025

the substitution of different cations alters the magnetic interactions between the Fe^{3+} ions, thereby modifying the material's coercivity, permeability, and magnetization[20], [21], [22].

Annealing temperature is one of the most critical factors influencing the structural, morphological, and magnetic properties of ferrite nanoparticles. Thermal treatment affects phase purity, crystallite size, grain growth, and defect density, which in turn impact the functional performance of the material[23], [24], [25]. Controlled annealing can enhance the crystallinity, reduce structural defects, and modify magnetic properties by altering the cation distribution within the spinel lattice. However, excessive annealing may lead to grain coalescence, which can degrade the material's performance in specific applications.

The sol-gel method is a widely used technique for synthesizing ferrite nanoparticles due to its advantages such as uniform mixing, low processing temperature, and high chemical homogeneity[5], [15], [16], [26], [27], [28], [29]. This method enables precise control over particle size and morphology, which are crucial for optimizing the magnetic and electrical properties of ferrites. In this study, Mg-Ni-Zn ferrite nanoparticles were synthesized via the sol-gel method and subjected to different annealing temperatures (200°C, 400°C, and 600°C) to investigate the resulting changes in structural, morphological, and magnetic properties. The primary objective of this research is to optimize the annealing conditions to achieve desired magnetic and structural characteristics for potential technological applications[30], [31].

EXPERIMENTAL METHODOLOGY

Synthesis of Mg-Ni-Zn Ferrite Nanoparticles

The nanoparticles were synthesized using the sol-gel method. Stoichiometric formula $Mg_{0.5-x}\ Ni_{0.2}\ Zn_{0.5}\ Fe_2O_4$ for x=0.2 of $Mg(NO_3)_2$, $Ni(NO_3)_2$, $Zn(NO_3)_2$, and $Fe(NO_3)_3$ were dissolved in de-ionized water and mixed with citric acid as a chelating agent. The solution was continuously stirred at 80°C to form a homogeneous solution, followed by the addition of ammonia to adjust the pH to ~7. The solution was then heated to form a gel, which was subsequently dried at 120°C to remove excess moisture. The dried precursor was subjected to pre-calcination at 200°C to decompose organic residues and obtain ferrite powder.

Annealing Process

The dried precursor was divided into multiple samples and annealed at temperatures of 200°C, 400°C, and 600°C for 2 hours in a muffle furnace. The gradual increase in temperature was maintained to avoid abrupt structural changes and ensure uniform phase formation. The annealed samples were then cooled naturally to room temperature inside the furnace.

For X=0.2

Chemical Reaction:

$0.3Mg(NO_3)_2.6H_2O + 0.2Ni(NO_3)_2.6H_2O + 0.5Zn(NO_3)_2.6H_2O + 2Fe(NO_3)_3.9H_2O + 3C_6H_8O_7 \rightarrow (Mg_{0.3}\ Ni_{0.2}\ Zn_{0.5}\ Fe_2O_4) + 4N_2\uparrow + 18CO_2\uparrow + 36H_2O$

RESULTS AND DISCUSSION

Structural Analysis

Figure 1 shows the XRD patterns of composition of $Mg_{0.5-x}Ni_xZn_{0.5}Fe_2O_4$ (where x = 0.2) for 200^0, 400^0 and 600^0C. The study of XRD patterns shows that all the prepared samples are single phase spinel cubic structure.The major diffraction peaks were observed at 2θ values of approximately 30.1°, 35.5°, 43.1°, 53.4°, 57.0°, and 62.6°, corresponding to the (220), (311), (400), (422), (333), and (440) planes, respectively. It is found that the Bragg's angles of corresponding peaks in the XRD pattern approximately matches with the characteristics of the reflection peaks of Mg- Ni- Zn ferrites which is reported in JCPDS number 08-0234.

ISSN No. 2454-6194 | DOI: 10.51584/IJRIAS |Volume X Issue VI June 2025

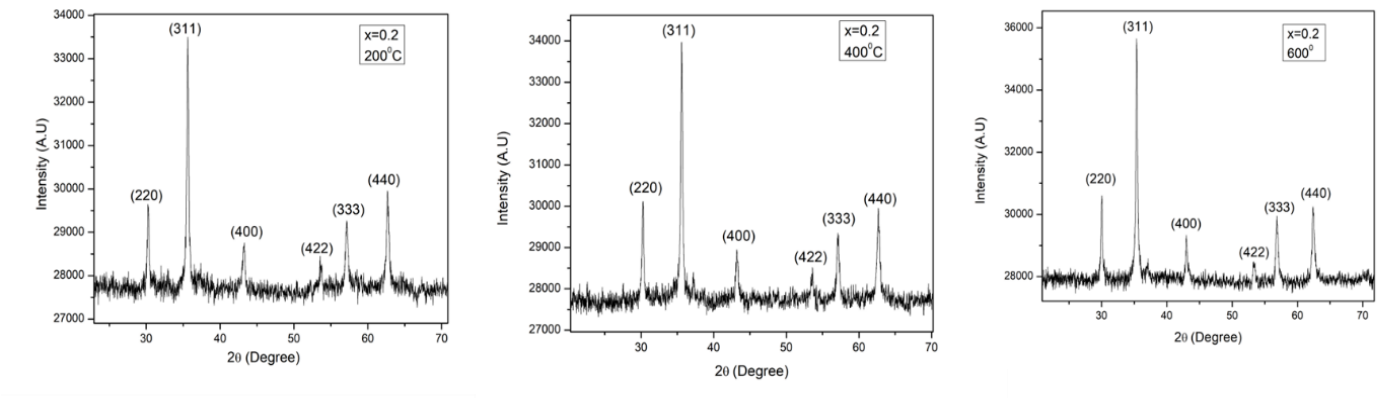

Fig.1: XRD of $Mg_{0.5-x}Ni_xZn_{0.5}Fe_2O_4$ nanoparticles for x = 0.2 for 200^0C, 400^0C and 600^0

Lattice constant

Lattice constant calculated by using formula $\frac{1}{d_{hkl}^2} = \frac{(h^2+k^2+l^2)}{a^2}$ it is found to be, 8.3591 Å for 200^0C, 8.3727 Å for 400^0C and 8.3963 Å for 600^0C. graph of temperature Vs lattice constant is shown in fig.2

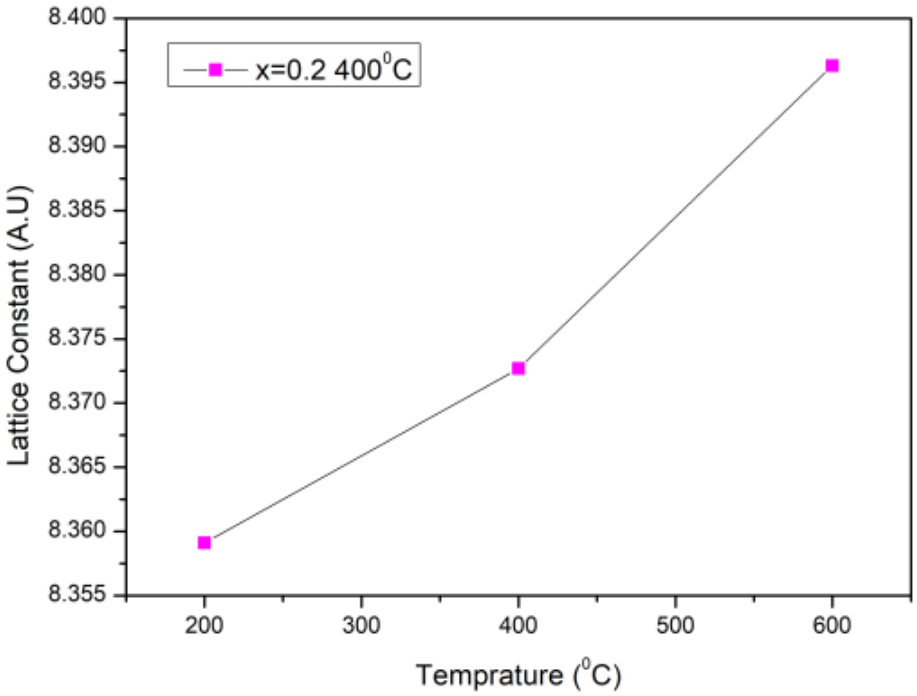

Fig. 2: Plot of temperature Vs lattice constant

Particle size

Particle size calculated by using Scherrer formula is 38 nm for 200^0C, 37 nm for 400^0C and 34 nm for 600^0C. Fig. shows the variation of particle size (t) with sintering temperature (T). From the graph it is seen that particle size decreases with increases in sintering temperature (T).

By using Scherrer formula particle size can be calculated, Scherrer formula given below;

$$D = \frac{0.9\,\lambda}{\beta\,cos\theta}$$

ISSN No. 2454-6194 | DOI: 10.51584/IJRIAS |Volume X Issue VI June 2025

Where, D : Particle size or Crystalline size

λ : Wavelength of X-ray in nm

β : Full width half maxima of peak

θ : Angle of peak

Unit of particle size is nanomaterials (nm).

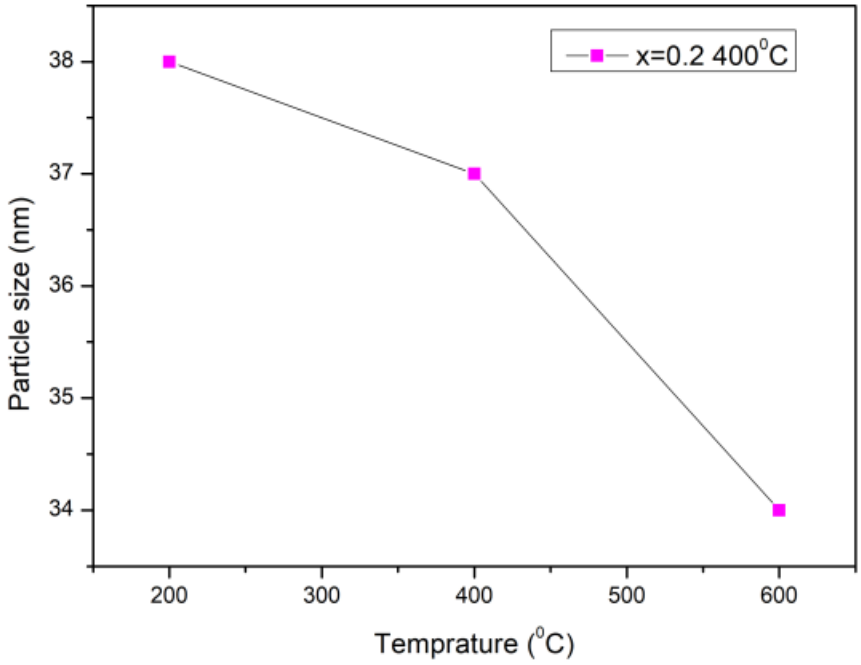

Fig. 3: Plot of temperature Vs Particle size

X-ray density

X-ray density calculated by using formula is 5.1728 Å for 200^{0}C, 5.1479 Å for 400^{0}C and 5.1046 Å for 600^{0}C. Fig. shows the variation of X-Ray density (D_x) with sintering temperature (T). From the graph it is seen that X-Ray density decreases with increases in sintering temperature (T).

X-ray density is calculated by using formula,

$$D_x = \frac{8\,M}{N_A a^3}$$

Where, D_x : X-ray density

M: molecular weight of the compound

N_A: Avogadro's number 6.022×10^{23}

8: Number of atom per unit cell

a: lattice constant

Unit of x-ray density is gm/cc.

ISSN No. 2454-6194 | DOI: 10.51584/IJRIAS |Volume X Issue VI June 2025

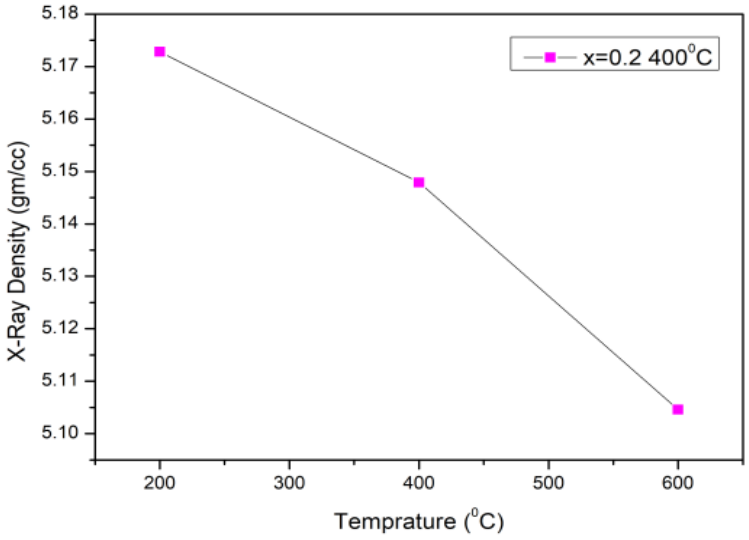

Fig. 4: Plot of temperature Vs x-ray density

Bond length

Bond length calculated by using formula is (A-O) site 1.8097 Å for 200^{0}C, 1.8126 Å for 400^{0}C and 1.8177 Å for 600^{0}C, for (B-O) site is 2.0897 Å for 200^{0}C, 2.0931 Å for 400^{0}C and 2.0990 Å for 600^0

The metal oxygen bond length (A-O) on tetrahedral site is calculated by using formula

$$A–O = (u – 0.25).a.\sqrt{3}$$

The metal oxygen bond length (B-O) on octahedral site is calculated by using formula

$$B–O = (0.625 – u)\ a$$

Where, u is recognized as oxygen ion parameter = $\frac{3}{8}$ = 0.375

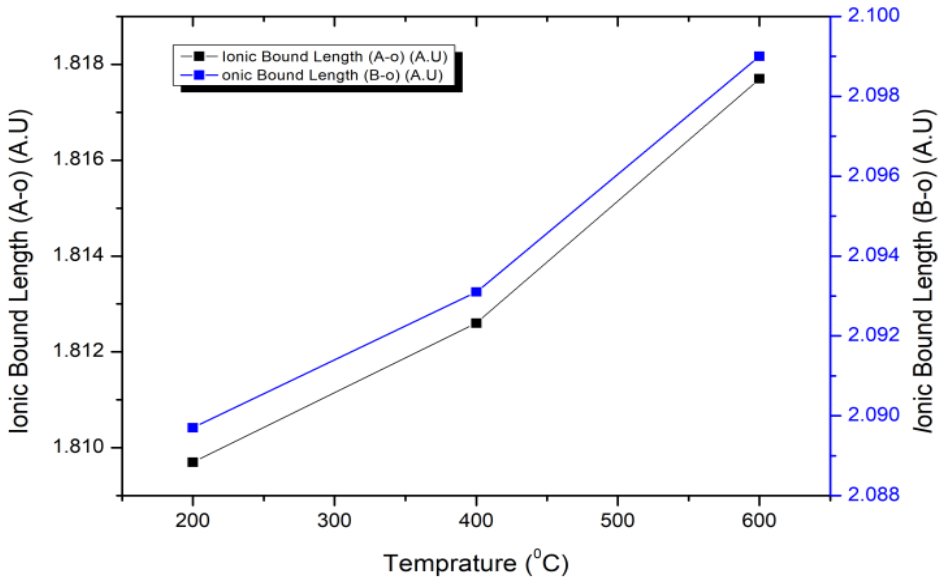

Fig. 5: Plot of temperature Vs Ionic bound length

ISSN No. 2454-6194 | DOI: 10.51584/IJRIAS |Volume X Issue VI June 2025

From the calculation, it is found that the bond length (B–O) of octahedral site is greater than the bond length of tetrahedral site (A–O) for all the composition. The bond length (A–O) and the bond length (B–O) is found to be increases with increases of sintering temperatures.

Ionic radii

Ionic radii calculated by using formula (R_A) site 0.4097 Å for 200^{0}C, 0.4126 Å for 400^{0}C and 0.4177 Å for 600^{0}C, for (R_B) site is) 0.6897 Å for 200^{0}C, 0.6911 Å for 400^{0}C and 0.6990 Å for 600^{0}C

From the calculations; it is found that the ionic radii R_A and R_B increases with increase in sintering temperature

Ionic radii in the tetrahedral site i.e., A-site and octahedral site i.e., B-site can be determined by using the formula given below:

$$R_A = [u - \frac{1}{4}]. a. 1.73 - r [O_2]^-$$

$$R_B = [\frac{8}{5} – u] a - r [O_2]^-$$

In which r $[O_2]^-$is the ionic radius of the oxygen atom having value 140 pm.

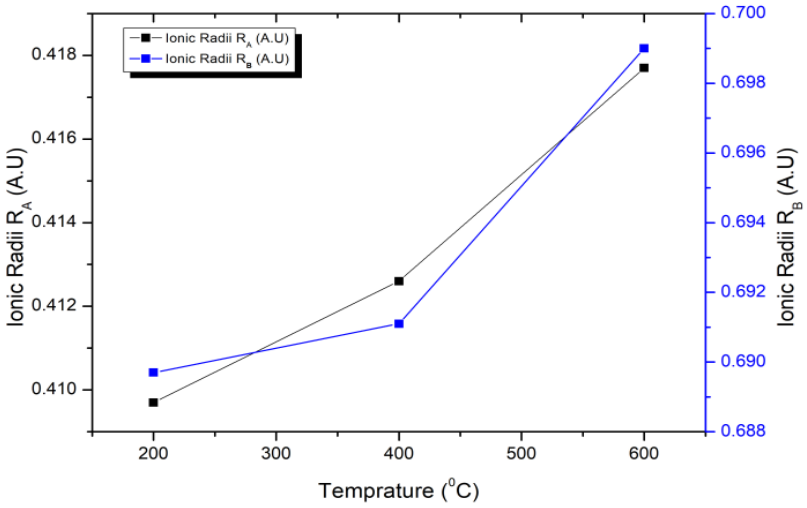

Fig. 6: Plot of temperature Vs ionic radii

Parameters calculated from XRD:

X	Temp. ^{0}C	Lattice Constant (a) A.U	X-Ray Density D_x gm/cc	Ionic Bond Length (A-O) A.U	Ionic Bond Length (B-O) A.U	Ionic Radii (R_A)A.U	Ionic Radii (R_B)A.U	Particle Size (t) nm
0.3	200	8.3591	5.1728	1.8097	2.0897	0.4097	0.6897	38
	400	8.3727	5.1479	1.8126	2.0931	0.4126	0.6911	37
	600	8.3963	5.1046	1.8177	2.099	0.4177	0.6990	34

Morphological Study

SEM images revealed that lower temperatures resulted in finer particles with irregular morphology and noticeable porosity, whereas higher temperatures led to well-defined grain growth and densification. At 600°C, particle aggregation was observed, leading to increased grain size and reduced porosity. The average grain size was estimated to be approximately 200nm at 200°C, 450 nm at 400°C, and 800nm at 600°C, showing a clear trend of grain coarsening with increasing temperature.

ISSN No. 2454-6194 | DOI: 10.51584/IJRIAS |Volume X Issue VI June 2025

Figure 7 shows the SEM image of prepared ferrite sample for sintering temperatures 200^{0}C, 400^{0}C and 600^{0}C.

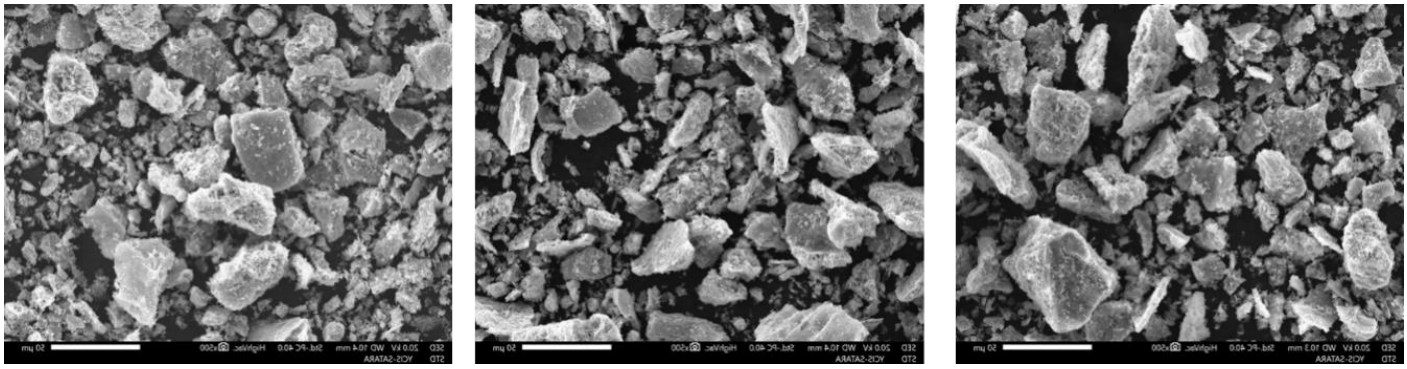

Fig.7: EDAX of $Mg_{0.5-x}Ni_xZn_{0.5}Fe_2O_4$ nanoparticles for x = 0.2 for 200^{0}C, 400^{0}C and 600^{0}C

EDS Analysis

Figure 9 shows the EDAX spectra of Mg-Ni-Zn ferrite for the sintering temperatures 200^{0}C, 400^{0}C and600^{0}C. The study of EDAX is done for the confirmation of metals used for the preparation of the sample.

Energy-dispersive X-ray spectroscopy (EDS) confirmed the successful incorporation of Mg, Ni, Zn, Fe, and O in the expected stoichiometric ratios. Elemental mapping indicated uniform distribution of these elements, ensuring homogeneity of the synthesized nanoparticles. The absence of any additional impurity peaks further validated the purity of the synthesized ferrite phase. Variations in elemental composition at different annealing temperatures were minimal, indicating that the thermal treatment did not lead to significant volatilization or loss of key elements.

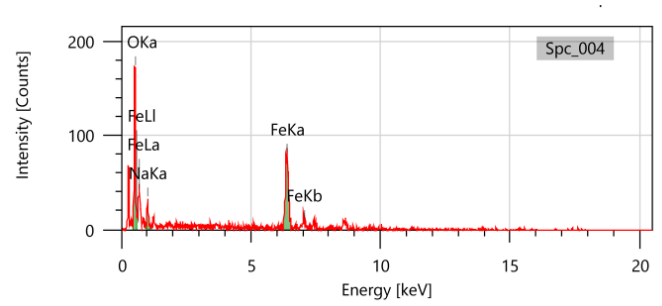

Display name	Standard data	Quantification method	Result Type
Spc_004	Standardless	ZAF	Metal

Element	Line	Mass%	Atom%
O	K	33.13±1.08	59.09±1.92
Na	K	9.24±1.10	11.46±1.37
Fe	K	57.63±2.22	29.45±1.13
Total		100.00	100.00
Spc_004			Fitting ratio 0.3264

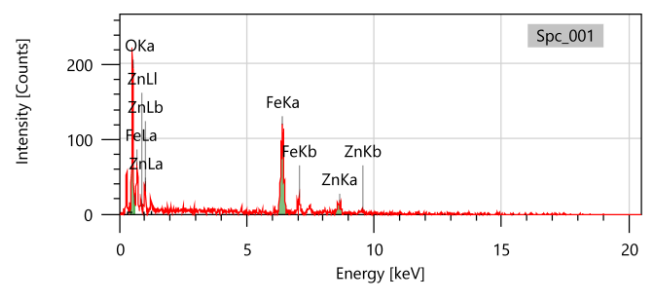

Display name	Standard data	Quantification method	Result Type
Spc_001	Standardless	ZAF	Metal

Element	Line	Mass%	Atom%
O	K	30.43±0.89	61.19±1.80
Fe	K	54.45±1.76	31.36±1.01
Zn	K	15.12±1.47	7.44±0.73
Total		100.00	100.00
Spc_001			Fitting ratio 0.2470

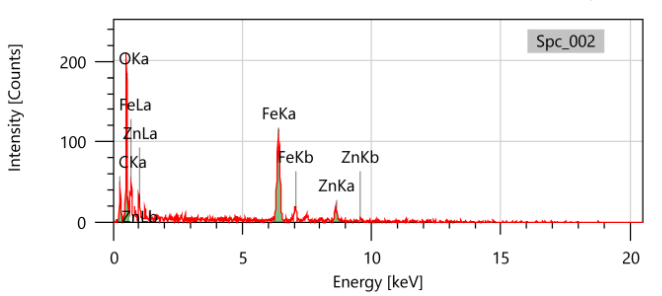

Display name	Standard data	Quantification method	Result Type
Spc_002	Standardless	ZAF	Metal

Element	Line	Mass%	Atom%
C	K	15.88±0.64	31.29±1.25
O	K	32.04±0.97	47.40±1.44
Fe	K	39.83±1.35	16.88±0.57
Zn	K	12.26±1.17	4.44±0.42
Total		100.00	100.00
Spc_002			Fitting ratio 0.1778

Fig.9: EDAX Pattern of $Mg_{0.5-x}Ni_xZn_{0.5}Fe_2O_4$ (where x = 0.2) for 200^{0}C, 400^{0}C and 600^{0}C

By using EDAX; compositional study of Mg-Ni-Zn ferrite was investigated. According to EDAX data, the precursors used for preparation of sample shows in appropriate amount. No any foreign element was found in the present compound. The elements detected in EDAX data are in good agreement with the elements used for the preparation of the sample. The presence of Mg, Ni, Zn, O and Fe was determined by their corresponding peaks.

VSM Analysis

Vibrating Sample Magnetometry (VSM) was employed to investigate the magnetic properties of the Mg-Ni-Zn ferrite nanoparticles. The magnetization curves exhibited characteristic hysteresis loops, indicating ferrimagnetic behaviour. The saturation magnetization (Ms) was found to increase with annealing temperature, reaching a maximum at 600°C. The coercivity (H_c) initially decreased with increasing temperature due to improved crystallinity and reduced strain, followed by a slight increase at higher temperatures due to grain coarsening effects. The remanence magnetization (Mr) also showed an increasing trend, suggesting enhanced magnetic interactions within the ferrite matrix. These results confirm that annealing plays a crucial role in tailoring the magnetic properties of Mg-Ni-Zn ferrite nanoparticles for various technological applications.

The magnetic characteristic of $Mg_{0.5-x}Ni_xZn_{0.5}Fe_2O_4$ nanoparticles for x = 0.2 for different sintering temperature such as 200^0C, 400^0C and 600^0C were carried by using Vibrating Sample Magnetometer (VSM) at room temperature.

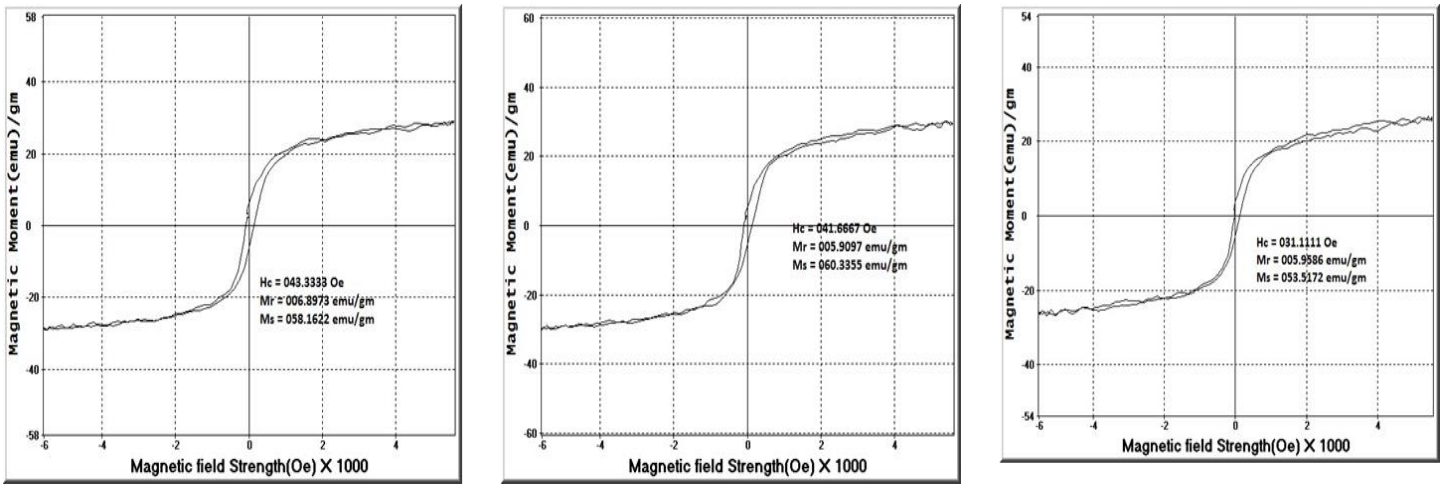

Fig.10: VSM of $Mg_{0.5-x}Ni_xZn_{0.5}Fe_2O_4$ nanoparticles for x = 0.2 for 200^0C, 400^0C and 600^0C

Parameters from Hysteresis loop for x=0.2

Parameter	150^0C	300^0C	450^0C
Coercive Force (H_c)	040.5556	046.1111	647.7778
Saturation remanent magnetization (M_r)	001.0752	004.0222	007.8000
Saturation magnetization (M_s)	038.7426	061.2000	061.3778

CONCLUSION

The study demonstrates the significant impact of annealing temperature on the structural, morphological, and magnetic properties of Mg-Ni-Zn ferrite nanoparticles synthesized via the sol-gel method. XRD analysis confirmed enhanced crystallinity and increased crystallite size with higher annealing temperatures. SEM analysis revealed grain growth and reduced porosity at elevated temperatures. EDS analyses validated the formation of the spinel phase and confirmed the expected elemental composition. VSM measurements indicated an increase in saturation magnetization and remanence with temperature, demonstrating the tunability of magnetic properties through controlled annealing. These findings provide valuable insights for optimizing the thermal treatment of ferrite nanoparticles to achieve desired structural and magnetic characteristics for potential applications in electronic and magnetic devices.

REFERENCES

1. M. Chaitanya Varma, S. Bharadwaj, G. S. V. R. K. Choudary, K. S. R. Murthy, and K. H. Rao, "Influence of magnesium-substituted Ni-Zn ferrites on magnetic and electric losses at lower frequency," *Int. J. Mod. Phys. B*, vol. 31, no. 9, 2017, doi: 10.1142/S0217979217500631.
2. Y. Hong *et al.*, "Magnetic, electrical, and structural properties of Mg2+-doped nickel–zinc ferrite prepared by sol–gel–SHS method," *J. Mater. Sci. Mater. Electron.*, vol. 31, no. 19, pp. 16975–16982, 2020, doi: 10.1007/s10854-020-04254-1.
3. R. B. Sathe, C. U. Narayankar, R. P. Patil, R. H. Patil, and S. B. Patil, "Investigation of structural and magnetic properties of novel Zn-substituted Ni–Mg ferrites," *J. Mater. Sci. Mater. Electron.*, vol. 34, no. 6, 2023, doi: 10.1007/s10854-022-09786-2.
4. B. B. Dora, S. Kumar, and M. C. Sahu, "Aloe vera Extract Solution," vol. 29, no. 53, pp. 307–311, 2014.
5. P. S. Kumar, G. K. S. Yadav, and V. K. V. Krishna, "P. S. Kumar," vol. 17, no. 2, pp. 191–199, 2021.
6. S. Satheeskumar, K. Ramesh, and N. inivasan, "Exploration of synthesis, Structural, Morphology and antibacterial activity of zn1-x-y mgx aly o nano particles," *Dig. J. Nanomater. Biostructures*, vol. 9, no. 4, pp. 1323–1330, 2014.
7. S. Thomas, G. Zaikov, Valsaraj, and Meera, "Nanoparticles: Synthesis, Characterization, and Applications," *Recent Adv. Polym. Nanocomposites Synth. Characterisation*, vol. 4, no. 3, pp. 7–24, 2020, doi: 10.1201/b12170-2.
8. R. Samal, M. Kandasamy, B. Chakraborty, and C. S. Rout, "Experimental and theoretical realization of an advanced bifunctional 2D δ-MnO2 electrode for supercapacitor and oxygen evolution reaction via defect engineering," *Int. J. Hydrogen Energy*, vol. 46, no. 55, pp. 28028–28042, 2021, doi: 10.1016/j.ijhydene.2021.06.054.
9. R. Sridhar, D. Ravinder, and K. V. Kumar, "Synthesis and Characterization of Copper Substituted Nickel Nano-Ferrites by Citrate-Gel Technique," *Adv. Mater. Phys. Chem.*, vol. 02, no. 03, pp. 192–199, 2012, doi: 10.4236/ampc.2012.23029.
10. N. Erfaninia, R. Tayebee, E. L. Foletto, M. M. Amini, M. Dusek, and F. M. Zonoz, "Preparation of magnetically recyclable ZnFe2O4 nanoparticles by easy single-step co-precipitation method and their catalytic performance in the synthesis of 2-aminothiophenes," *Appl. Organomet. Chem.*, vol. 32, no. 2, pp. 1–7, 2018, doi: 10.1002/aoc.4047.
11. Â. M. L. Denadai *et al.*, "Self-assembled organic-inorganic magnetic hybrid adsorbent ferrite based on cyclodextrin nanoparticles," *Beilstein J. Org. Chem.*, vol. 8, pp. 1867–1876, 2012, doi: 10.3762/bjoc.8.215.
12. B. Baburao and D. Ravinder, "Development of rare-earth doped nano-ferrites for Industry applications," *Int. J. Eng. Res. Appl. www.ijera.com*, vol. 11, no. 3, pp. 13–17, 2021, doi: 10.9790/9622-1103021317.
13. D. Nath and D. A. Arunkumar, "A Study of Electrical and Magnetic Properties of Nano Ferrites," *Ijireeice*, vol. 10, no. 3, pp. 112–117, 2022, doi: 10.17148/ijireeice.2022.10319.
14. T. Dippong, *Characterization and applications of metal ferrite nanocomposites*, vol. 12, no. 1. 2022. doi: 10.3390/nano12010107.
15. J. Massoudi *et al.*, "Magnetic and spectroscopic properties of Ni-Zn-Al ferrite spinel: From the nanoscale to microscale," *RSC Adv.*, vol. 10, no. 57, pp. 34556–34580, 2020, doi: 10.1039/d0ra05522k.
16. H. Dubey, C. Verma, U. Rai, A. Kumar, and P. Lahiri, "Synthesis, characterization and properties of nickel based zinc ferrite nanoparticles," *Indian J. Chem. -Section A*, vol. 58, no. 04, pp. 454–458, 2019.
17. M. F. Nanoparticles, "Structural and FTIR Spectroscopic Studies of Mg-Zn Ferrite Nanoparticles Synthesized by Co-Precipitation Technique," *Int. J. Sci. Res.*, vol. 5, no. 2, pp. 1524–1528, 2016, doi: 10.21275/v5i2.nov161491.
18. G. S. Shahane, A. Kumar, M. Arora, R. P. Pant, and K. Lal, "Synthesis and characterization of Ni-Zn ferrite nanoparticles," *J. Magn. Magn. Mater.*, vol. 322, no. 8, pp. 1015–1019, 2010, doi: 10.1016/j.jmmm.2009.12.006.
19. A. S. Džunuzović *et al.*, "Structure and properties of Ni-Zn ferrite obtained by auto-combustion method," *J. Magn. Magn. Mater.*, vol. 374, pp. 245–251, 2015, doi: 10.1016/j.jmmm.2014.08.047.
20. H. R. Ebrahimi, M. Parish, G. R. Amiri, B. Bahraminejad, and S. Fatahian, "Synthesis, characterization

and gas sensitivity investigation of Ni0.5Zn0.5Fe2O4 nanoparticles," *J. Magn. Magn. Mater.*, vol. 414, pp. 55–58, 2016, doi: 10.1016/j.jmmm.2016.04.043.

21. A. V. Knyazev, I. Zakharchuk, E. Lähderanta, K. V. Baidakov, S. S. Knyazeva, and I. V. Ladenkov, "Structural and magnetic properties of Ni-Zn and Ni-Zn-Co ferrites," *J. Magn. Magn. Mater.*, vol. 435, pp. 9–14, 2017, doi: 10.1016/j.jmmm.2017.03.074.
22. X. Zhou, J. Wang, L. Zhou, Y. Wang, and D. Yao, "Structure, magnetic and microwave absorption properties of NiZnMn ferrite ceramics," *J. Magn. Magn. Mater.*, vol. 534, no. April, p. 168043, 2021, doi: 10.1016/j.jmmm.2021.168043.
23. R. S. Kawale, "CU-ZN FERRITE NANOPARTICLES SYNTHESIZED WITH GREEN TEA EXTRACT," vol. 11, no. 12, pp. 3551–3557, 2022.
24. I. Sharma and E. Garg, "A review on nanoferrites in biomedical applications," *Ijbas*, vol. 11, no. 2, p. 16, 2022, doi: 10.13140/RG.2.2.27151.2.
25. B. R. Babu, B. B. V. S. V. Prasad, and M. S. R. Prasad, "Study of electrical and magnetic properties of Ni - Zn - Mg ferrite system," *Mod. Phys. Lett. B*, vol. 28, no. 31, pp. 1–10, 2014, doi: 10.1142/S0217984914502443.
26. S. Guan *et al.*, "A review of the preparation and applications of MnO2 composites in formaldehyde oxidation," *J. Ind. Eng. Chem.*, vol. 66, pp. 126–140, Oct. 2018, doi: 10.1016/j.jiec.2018.05.023.
27. R. N. Reddy and R. G. Reddy, "Synthesis and electrochemical characterization of amorphous MnO2 electrochemical capacitor electrode material," *J. Power Sources*, vol. 132, no. 1–2, pp. 315–320, 2004, doi: 10.1016/j.jpowsour.2003.12.054.
28. D. D. Kulkarni, V. R. Joshi, S. N. Shetty, S. B. Patel, and M. S. Khalfe, "Comparative Study between Co-Precipitation and Sol Gel Method for the Preparation of Ferrites," vol. 2, no. 4, pp. 169–176, 2022, doi: 10.48175/IJARSCT-3467.
29. P. Badanayak, J. V Vastrad, and C. Author, "Sol-gel process for synthesis of nanoparticles and applications thereof," *Pharma Innov. J.*, vol. 10, no. 8, pp. 1023–1027, 2021, [Online]. Available: http://www.thepharmajournal.com
30. M. M. Kothawale, "Literature Survey on Nano Ni-Zn Ferrite Material," vol. 6, no. 1, pp. 676–680, 2019.
31. B. Ünal, S. Ünver, H. Güngüneş, U. Topal, A. Baykal, and H. Sözeri, "Microwave, dielectric and magnetic properties of Mg-Ti substituted Ni-Zn ferrite nanoparticles," *Ceram. Int.*, vol. 42, no. 15, pp. 17317–17331, 2016, doi: 10.1016/j.ceramint.2016.08.028.